CHD_3 Dissociation on Pt(111): A Comparison of the Reaction Dynamics Based on the PBE Functional and on a Specific Reaction Parameter Functional

H. Chadwick[a),b)], D. Migliorini[a)] and G.J. Kroes

Leiden Institute of Chemistry, Gorlaeus Laboratories, Leiden University, P.O. Box 9502, 2300 RA Leiden, The Netherlands

We present a comparison of *ab-initio* molecular dynamics calculations for CHD_3 dissociation on Pt(111) using the PBE functional and a specific reaction parameter (SRP) functional. Despite the two functionals predicting approximately the same activation barrier for the reaction, the calculations using the PBE functional consistently overestimate the experimentally determined dissociation probability whereas the SRP functional reproduces the experimental values within chemical accuracy (4.2 kJ/mol). We present evidence that suggests that this difference in reactivity can at least in part be attributed to the presence of a van der Waals well in the potential of the SRP functional which is absent from the PBE description. This leads to the CHD_3 molecules being accelerated and spending less time near the surface for the trajectories run with the SRP functional, as well as more energy being transferred to the surface atoms. We suggest that both these factors reduce the reactivity observed in the SRP calculations compared to the PBE calculations.

a) H. Chadwick and D. Migliorini contributed equally to this work

b) Email: h.j.chadwick@lic.leidenuniv.nl

I. INTRODUCTION

The dissociation of methane on a transition metal catalyst is one of the rate controlling steps in the steam reforming reaction[1], used for the commercial production of hydrogen. Developing an accurate predictive understanding of this industrially important reaction is of potentially great value, and could provide a method of improving the catalyst rather than relying on trial and error. Quantum-state resolved reactivity measurements[2–5] have shown that the dissociation of methane is mode-specific, i.e. the initial dissociation probability, or sticking coefficient, depends not only on the total energy of the methane, but also how the energy is distributed among the degrees of freedom of the molecule[6–9]. Additionally, in partially deuterated methanes, the C-H bond can be selectively broken by adding a quantum of C-H stretch vibration to the molecule[6,10,11]. The reaction has also been shown to be stereospecific[12,13] and site-selective[14]. The above observations mean that the dissociative chemisorption of methane on transition metal surfaces cannot be accurately described using statistical theories[15]. Several groups[16–22] have used dynamical methods to describe the dissociation of methane on transition metal surfaces all of which rely on density functional theory (DFT) to calculate the potential energy of the system.

For interactions at the gas-surface interface, generalized gradient approximation (GGA) exchange-correlation functionals are typically used. Even for reactions in the gas-phase, these functionals have a mean unsigned error of 3.8 kcal/mol (15.9 kJ/mol)[23] well above the 1 kcal/mol (4.2 kJ/mol) limit which is considered to define chemical accuracy. This value has not been determined for gas-surface reactions, but using DFT with the most common GGA functionals fails to predict the activation barrier (E_b) for dissociation within chemical accuracy[24]. An alternative semi-empirical method is to mix two GGA functionals, one which overestimates E_b and one which underestimates the reaction barrier, to create a specific reaction parameter (SRP) functional[25,26]. For gas-surface reactions, PBE[27] and PW91[28] typically underestimate E_b and RPBE[29] tends to overestimate E_b[26,30–36]. Combining these to make an SRP functional can produce chemically accurate results for gas-surface reactions, as was first demonstrated by mixing the PW91[28] and

RPBE[29] functionals for H_2 on Cu(111)[26,37] and Cu(100)[30]. We have also demonstrated that an SRP exchange correlation functional can be used to reproduce the experimental sticking coefficients for CHD_3 on Ni(111) for both molecules prepared with a quantum of C-H stretch vibration and those without vibrational excitation[22]. The same SRP functional, which uses the RPBE[29] and PBE[27] for exchange and van der Waals for correlation[38], was also shown to give chemically accurate results for the sticking coefficients for CHD_3 dissociation on Pt(111) and Pt(211)[39], demonstrating the transferability of the SRP functional among systems in which methane reacts with group 10 transition metals of the periodic table, and also from a flat to a stepped transition metal surface. In recent work, the same SRP functional has been shown to accurately describe site-specific reactivity by reproducing the sticking coefficients for the dissociation of CH_4 on the step sites of Pt(211)[14].

For the dissociation of methane on Pt(111) the PBE and SRP functionals both predict the same E_b for the reaction, to within 1 kJ/mol. Despite this, and as we will show, the PBE functional considerably overestimates the experimentally determined sticking coefficients for CHD_3 on Pt(111), whereas the SRP functional reproduces the measurements within chemical accuracy. The inclusion of the van der Waals correlation in the SRP functional reproduces the physisorption well which is present in the system[40] but is absent from the PBE description as discussed more in Section III. Previous work by Jackson and co-workers using their Reaction Path Hamiltonian model presented in the Supporting Information of Ref. 39 has suggested that the coupling of translational motion along the minimum energy path (MEP) to vibrational motion is larger with the SRP functional than the PBE functional due to the presence of the van der Waals well. The effect of this may be to remove energy from motion along the MEP and convert it to motion away from the MEP, reducing the observed reactivity with the SRP functional. Similar arguments have also been presented to explain why vibrational energy can promote the dissociation of methane on transition metal surfaces more than the same amount of translational energy, i.e. the vibrational efficacy can be more than 1[7,41–45]. The vibrationally excited molecules stay closer to the MEP than the molecules with only translational energy meaning they sample parts of the potential energy surface (PES) with

a lower E_b. This can lead to an increase in reactivity which is more than would be anticipated by the amount of vibrational energy added[7].

Another effect of including the van der Waals correlation could be to change the energetic corrugation of the PES i.e. how the shape of the PES changes with motion parallel to the plane of the surface. A recent study[35] compared several density functionals for the dissociation of H_2 on Ru(0001) and found that those which included a van der Waals correlation better reproduced the dependence of experimentally determined sticking coefficients on incident translational energy than functionals which did not include van der Waals correlation. As the gradient of the sticking coefficient curve reflects the distribution of activation barrier heights present on the surface, this was attributed to functionals that included van der Waals correlation providing a better description of the energetic corrugation than functionals without van der Waals correlation.

In this paper, we will present a detailed comparison of the results from *ab-initio* molecular dynamics (AIMD) calculations performed using the SRP and PBE functionals to further investigate why they predict such different reactivity for the dissociation of CHD_3 on Pt(111). The rest of the paper is organized as follows. In Section II we give an overview of the theoretical methods used in the current work, before presenting the results and discussion in Section III. Section IV presents a summary of the key points.

II. METHODS

The theoretical methods employed in the current work have been described in detail previously[22,39] and only the most relevant aspects will be presented here. In brief, we ran between 500 and 1000 quasi-classical trajectories for CHD_3 colliding with Pt(111) for a range of incident energies using the Vienna *ab-initio* simulation package (VASP) version 5.3.5[46–49]. The first Brillouin zone has been sampled using a 4x4x1 Γ-centered grid and the cut off energy for the plane wave basis set was 350 eV. Projector augmented wave pseudopotentials[50,51] have been used to represent the core electrons. For the SRP calculations, the same pseudopotentials have been used

consistently throughout the calculations, whereas for the PBE calculations a different Pt pseudopotential was used for equilibrating the surface and in the AIMD trajectory calculations. As discussed in more detail in the Supplementary Material, the maximum error this introduces in the E_b for the reaction calculated using the PBE functional is 0.4 kJ/mol which is not significant enough to change the results of the PBE trajectories presented here. The Pt(111) surface has been modelled using a 5 layer (3x3) supercell slab[36,39] with each slab separated from its first periodic replica by 13 Å of vacuum. A 0.1 eV Fermi smearing has been used to facilitate the convergence. Extensive tests of the parameters used in the calculations have been performed, the results of which can be found in the Supporting Information of Ref. 39.

The PBE[27] and the SRP functional developed in Ref. 22 have been used in the DFT calculations. The SRP exchange-correlation functional (E_{XC}^{SRP}) is defined as

$$E_{XC}^{SRP} = (1-x)E_X^{PBE} + xE_X^{RPBE} + E_C^{vdW} \quad (1)$$

where E_X^{PBE} and E_X^{RPBE} are respectively the PBE[27] and RPBE[29] exchange functionals, and E_C^{vdW} is the van der Waals correlation functional[38]. Previous work[39] has shown that $x = 0.32$ produces chemically accurate results for the dissociation of CHD_3 on Pt(111) and we will use this value of x here. We will refer to this SRP functional as SRP32-vdW.

The initial conditions used for the trajectory calculations were sampled to replicate the molecular beam scattering experiments of Beck and co-workers presented in Ref. 39. For the 'laser-off' trajectories, the vibrational populations of the molecules were sampled using a Boltzmann distribution at the nozzle temperature used to create the molecular beam expansion, whereas for the $v_1 = 1$ calculations, all the molecules were prepared with a single quantum of C-H stretch vibration. The translational energies of the molecules in each case were sampled from the experimental time of flight distribution, and the positions and velocities of the surface atoms from dynamics calculations run to equilibrate the bare slab at a surface temperature of 500 K. More details about the sampling of the molecular initial conditions can be found in the Supporting Information of References 22 and 39.

At the start of the trajectory, the CHD_3 is positioned 6 Å above the surface with x and y chosen to randomly sample all the positions on the Pt(111) slab. The trajectories were propagated with a time step of 0.4 fs using the velocity-Verlet algorithm until the CHD_3 either dissociated on the Pt(111) surface, or scattered back into the gas phase. The molecule was considered to have reacted if one of the bonds in the molecule was greater than 3 Å, whereas if the center of mass (COM) of the molecule was 6 Å away from the surface with the COM velocity directed away from the surface it was considered to have been scattered[39]. All the trajectories were found to either react or scatter within the maximum 1 ps timeframe that the trajectory was propagated for; we observed that no molecules remained trapped on the surface.

The sticking coefficients, S_0, were calculated from the AIMD calculations using

$$S_0 = \frac{N_{\mathrm{react}}}{N_{\mathrm{tot}}} \tag{2}$$

where N_{react} is the number of trajectories that dissociate and N_{tot} is the total number of trajectories. The statistical error bars were found as

$$\sigma = \sqrt{\frac{S_0(1-S_0)}{N_{\mathrm{tot}}}} \tag{3}$$

and represent 68% confidence limits.

III. RESULTS AND DISCUSSION

The sticking coefficients calculated from the AIMD trajectories using the PBE functional (green) are compared with those obtained experimentally[39] (red) in Fig. 1, for molecules under laser-off conditions (panel A), and those prepared with a single quantum of C-H stretch (panel B). The calculated S_0 are seen to systematically overestimate the values that have been measured both with and without laser excitation. To quantify the extent to which the PBE functional overestimates S_0, the experimental data were fit to an S-shape curve using

$$\mathrm{S}_0(E_i) = \frac{A}{2}\left(1 + \mathrm{erf}\left(\frac{E_i - E_0}{W}\right)\right) \tag{4}$$

where A is the value of S_0 at infinitely high translational energy, E_i is the incident energy, E_0 is the average activation barrier height for the dissociation and W is the width of the distribution of barrier heights. The energy shift between the fit to the experimental data and the S_0 determined using the PBE functional could then be found, with the values (in kJ/mol) also presented in Fig. 1. Not including the two highest energy laser-off and $v_1 = 1$ points calculated as these fall outside the range of the experimentally determined S_0, the average energy shift between the two sets of data is 13.1 kJ/mol. This is over a factor of 3 higher than the 4.2 kJ/mol (1 kcal/mol) which is typically considered to define chemical accuracy.

In Fig. 2, the S_0 calculated from AIMD trajectories using the PBE functional (green) are compared with those obtained using the SRP32-vdW functional[39] (blue). Again, the results using the PBE functional are larger than those obtained using the SRP32-vdW functional. Using the same analysis as described above, the average energy shift between the PBE and the SRP32-vdW functional is 13.9 kJ/mol, where the highest two energy PBE points have not been included in the average as the energy shifts have to be determined by extrapolating the SRP32-vdW fit outside the E_i range where values of S_0 have been determined. This result might suggest that the PBE functional would give an activation barrier which is approximately 14 kJ/mol lower in energy than the SRP32-vdW functional. However, as shown in Table I, the values of the E_b obtained from the PBE and SRP32-vdW functional are almost the same (differing by no more than 1 kJ/mol) both with and without zero point energy corrections.

TABLE I. The activation barriers (E_b) and zero point energy corrected activation barriers (E_b^c) for the dissociation of CHD_3 on Pt(111) calculated using the SRP32-vdW, PBE and RPBE density functionals.

Functional	SRP32-vdW	PBE	RPBE[36]
E_b (kJ/mol)	78.6	78.0	112.8
E_b^c (kJ/mol)	66.5	66.1	100.9

Whilst the activation barriers for the dissociation calculated with the SRP32-vdW and PBE functionals are similar, an important difference between the two functionals is that the SRP32-vdW

description includes a van der Waals well whereas the PBE does not, as shown by the one dimensional cuts through the PESs in Fig. 3. As the SRP32-vdW functional predicts the experimental S_0 within chemical accuracy unlike the PBE functional, we compared the dynamics obtained using the two functionals to determine to what extent the differences in the reactivity can be attributed to the presence of the van der Waals well in the SRP32-vdW description, or to other topological features of the PES. Specifically we have investigated the effect of surface motion on the effective activation barrier height, how closely the trajectories that dissociate follow the minimum energy path, how significant the acceleration of the SRP32-vdW trajectories due to the van der Waals well on approach to the surface is and the extent to which energy is transferred from the molecules to the surface for the two functionals. Each of these will be addressed in turn in the sections below.

A. Surface Motion and Effective Barriers

The activation barriers presented in Table I were calculated for a frozen 0 K surface, whereas the AIMD calculations were run at a surface temperature of 500 K. Previous studies[19,52–56] have shown that the position of the transition state (TS) above the surface and the effective activation barrier height depend on the motion of the closest surface atom out of the plane of the surface making S_0 dependent on surface temperature. The height of the COM of the TS above the surface atom is presented in Fig. 4A for the PBE functional (green) and the SRP32-vdW functional (blue). Positive values of Q correspond to the surface atom closest to the methane being above the plane, negative Q to it being below the plane, and 0 to the atom being in the plane of the surface. The change in height of the TS with surface atom motion is similar for both functionals, with the mechanical coupling[57,58] $\alpha = \frac{\mathrm{d}Z_b}{\mathrm{d}Q}$ being 0.80 for the PBE functional, and $\alpha = 0.82$ for the SRP32-vdW functional, in reasonable agreement with previous results[57,59]. In the Equation for α, Z_b defines the distance of the TS to the macroscopic surface. The barrier height as a function of the out

of plane surface atom displacement under the dissociating CHD_3 is presented in Fig. 4B for the PBE functional (green) and the SRP32-vdW functional (blue). For both functionals, the barrier height increases as the surface atom moves into the bulk, and decreases as it moves above the plane. This effect is larger for the PBE functional, where the electronic coupling[57,58] $\beta = -\frac{dE_b}{dQ}$ is equal to 90.2 kJ/mol/Å. For the SRP32-vdW functional, β = 77.8 kJ/mol/Å. The same surface atom displacement therefore leads to a larger decrease in E_b for the PBE functional than for the SRP32-vdW functional.

The distribution of Q for each functional has been calculated by analyzing 1 ps of bare slab dynamics for ten different initial slabs, and the two distributions are presented in Fig. 4C for the PBE (green) and SRP32-vdW (blue) functionals. These have been obtained using Gaussian binning with a 0.01 Å bin size and a 0.05 Å broadening parameter. Both the distributions are centered close to 0 Å, but the distribution for the SRP32-vdW functional is slightly broader and shifted to more positive values of Q. From the activation barriers and the distribution of Q presented in Figs. 4B and 4C, the average activation barrier experienced by the CHD_3 in the calculations has been determined using

$$\langle E_b(Q) \rangle = \frac{\sum_{i=0}^{i_{\max}} P(Q_i)\, E_b(Q_i) \Delta Q_i}{\sum_{i=0}^{i_{\max}} P(Q_i)\, \Delta Q_i} \tag{5a}$$

$$Q_i = Q_{i=0} + i\, \Delta Q_i \tag{5b}$$

where $P(Q_i)$ is the probability of finding the surface atom displaced by Q_i, $E_b(Q_i)$ the value of the barrier for the displacement Q_i and $i = 0$ and $i_{\max}$ correspond to values of Q_i for which $P(Q_i)$ is negligible. The effective barriers calculated in this way are 76.6 kJ/mol and 76.2 kJ/mol for the PBE and SRP32-vdW functionals respectively, so that the difference between these barriers does not account for energy shift between the two curves presented in Fig. 2.

B. Motion Across the Potential Energy Surface and the Minimum Energy Path

Whilst the activation barrier for methane dissociation determined with the SRP32-vdW and PBE functionals are similar, dissociation does not necessarily occur via the lowest energy transition

state, and so other differences in the SRP32-vdW and PBE potentials could be responsible for the differences in reactivity predicted using the two functionals. Two-dimensional cuts through the PESs for the SRP32-vdW functional (panel A) and PBE functional (panel B) are presented in Fig. 5. These were calculated holding the internal co-ordinates of the molecule fixed in the TS geometry given in Table II for dissociation above a top site on the surface. In each plot, the MEP is shown as a white dotted line and the TS as a black square. The coordinate perpendicular to the MEP at the TS (χ) is reported as a dashed black line. As shown in Fig. S1 and Table SIII in the Supplementary Material, the curvature of the MEP for the SRP32-vdW PES is slightly larger than for the PBE functional as the turn in the MEP towards the TS for the SRP32-vdW functional is tighter. Figure S2 presents one dimensional cuts through the PES perpendicular to the MEP at the TS (along χ) for the SRP32-vdW (blue) and PBE (green) functionals. The curves have been shifted down by E_b for each functional so that the TS energy is at 0 kJ/mol. The saddle point in the SRP32-vdW PES is slightly wider than for the PBE PES, but not by much. As shown by the averaged properties of the reacted trajectories presented in Table SIV, the geometries of the trajectories that react are similar for the two functionals. From this we can conclude that the width of the saddle point at the TS is similar for the PBE and SRP32-vdW functionals, and small differences probably do not contribute to the different reactivity of the two functionals. There is also no evidence of significantly different energetic corrugation of the two PESs, as the average distance between the COM and a top site when the molecules dissociate (δ_{Top}) are similar (see Table SIV).

TABLE II. The dissociating bond length (r^{TS}), height of the carbon atom above the surface (Z_C^{TS}), angle between the dissociating bond and the surface normal (θ), angle between the umbrella axis and surface normal (β) and the angle between the umbrella axis and dissociating bond (γ) at the transition state for the SRP32-vdW functional (top row) and PBE functional (bottom row).

	r^{TS} (Å)	Z_C^{TS} (Å)	$\theta(^\circ)$	$\beta(^\circ)$	$\gamma(^\circ)$
SRP32-vdW	1.55	2.29	133	168	35
PBE	1.51	2.24	132	169	37

To quantify the extent to which the PBE and SRP32-vdW trajectories follow the MEP across the PES χ_r was calculated as the distance from the TS in r and Z when the trajectory crosses the χ coordinate

$$\chi_r = \sqrt{(Z_C - Z_C^{TS})^2 + (r - r^{TS})^2} \tag{6}$$

where Z_C is the height of the carbon above the surface, r the dissociating bond length and the quantities with a TS superscript are the corresponding transition state values. The angle between the dissociating bond and surface normal, θ, has not been included in this analysis as the values at the transition state, are very similar for both functionals as shown in Table II. Additionally, there is no significant difference in the distributions of θ for the trajectories that react, which are given in Table SIV of the Supplementary Material. $\langle\chi_r\rangle$ has been calculated for trajectories that begin within 0.1 Å, 0.2 Å, 0.3 Å, and 0.4 Å of a top site in the xy plane. The results are presented in Fig. 5C for the PBE (green) and SRP32-vdW (blue) trajectories, and the distributions of χ_r in Fig. S3. Additionally, the paths of the reactive trajectories that start within 0.1 Å of a top site for each functional are shown as brown lines in Figs. 5A and 5B. Whilst the analysis at 0.1 Å suggests that the SRP32-vdW trajectories follow the MEP less, the opposite trend is seen considering the trajectories that start further away from the top site. In this analysis, we therefore see no firm evidence of the 'bobsled effect'[60–62], where it would be expected that the SRP32-vdW trajectories which are accelerated by the van der Waals well and therefore moving faster, as shown in Figs. 6A, B and C, would go further up the repulsive wall of the PES and cross χ at more negative values of χ_r. The motion up the repulsive wall would also lead to an oscillation (a vibration) in the motion with respect to the MEP, and we find no evidence of increased vibrational excitation of the scattered SRP32-vdW trajectories compared to the PBE trajectories, as shown in Table SV (δE_{vib}). This is in contrast to an earlier suggestion presented in the Supporting Information of Ref. 39, where larger coupling constants were found between motion along the MEP to vibration for the SRP32-vdW functional than for the PBE functional using the Reaction Path Hamiltonian model,

which was attributed to the presence of the van der Waals well. However, the results from the AIMD trajectories presented here suggests the presence of the van der Waals well may not lead to increased energy transfer from translation to vibrations for the SRP32-vdW functional compared to the PBE functional.

C. Molecule-Surface Interaction Times

Although the van der Waals well accelerates the SRP32-vdW trajectories, the molecules arrive at the TS (black dashed line in Figs. 6A, B and C) with a similar velocity for both functionals. However, as the SRP32-vdW trajectories are accelerated, the time it takes to travel over a certain distance to the TS is less than for the PBE trajectories (green), as shown in Fig. 6D. The TS for the SRP32-vdW functional is also 0.05 Å further from the surface than for the PBE functional. All this means that the interaction time with the surface is shorter and the molecules have less time to distort towards the TS geometry, given in Table II, in the SRP32-vdW calculations. The TS also has a longer bond length (r) for the SRP32-vdW functional. The TS being later in r for the SRP32-vdW functional and the CHD_3 having less time to distort to the TS geometry will likely lead to the lower sticking coefficient observed in the SRP32-vdW calculations than in the PBE, although it is not easy to quantify by how much.

D. Energy Transfer to the Surface

The analysis of the scattered trajectories shows that the energy transfer to the surface is between 1 kJ/mol and 3 kJ/mol larger for the SRP32-vdW calculations than the PBE calculations. This difference can be explained qualitatively using the modified Baule model. The initial Baule model estimates the energy transfer (E_T^{Baule}) to the surface treating the molecule as a hard sphere colliding on a single surface atom[63]. For an incident energy E_i, E_T^{Baule} is given by

$$E_T^{Baule} = \frac{4\mu E_i}{(1+\mu)^2} \tag{7}$$

where μ is the mass ratio between the mass of CHD_3 and an effective surface mass M_S, often taken as the mass of a single Pt atom. The Modified Baule (M. Baule) model takes into account the additional kinetic energy the methane gains while travelling towards the surface due to the interaction with the surface. For an incident energy E_i

$$E_T^{M.\ Baule} = \frac{4\mu(E_i + E_{ads})}{(1+\mu)^2} \tag{8}$$

where E_{ads} is the molecular adsorption energy. The results for the Baule model (black) and for the Modified Baule model for the SRP32-vdW (blue) and PBE (green) functionals are compared with the energy transfer calculated from the AIMD trajectories (blue and green open symbols for SRP32-vdW and PBE respectively) in Fig. 7. The solid lines are straight line fits to the data.

For the Modfied Baule model ΔE_T reads

$$\Delta E_T = \frac{4\mu(E_{ads}^{SRP} - E_{ads}^{PBE})}{(1+\mu)^2} \tag{9}$$

where E_{ads}^{SRP} and E_{ads}^{PBE} are the largest molecular adsorption energies computed with the two functionals and are equal to 21.9 kJ/mol and 1.5 kJ/mol respectively. This is deeper than shown in Fig. 3 for the SRP32-vdW functional as the value here includes the residual energy correction of 4.0 kJ/mol as discussed in the Supporting Information of Reference 39. Using Eq. (9) gives a value of 6.6 kJ/mol, qualitatively reproducing the difference in energy transfer to the surface for the PBE and SRP32-vdW trajectories. This suggests that the difference in energy transfer can be attributed to the difference in E_{ads}.

We note that the actual amount of energy transferred to the surface in the reactive collisions may well be higher than that for scattered trajectories. Previous research has shown that CHD_3 reacts close to surface atoms, while scattered CHD_3 also samples surface sites away from the top sites (the positions of the surface atoms, see Fig. 2 of Ref. 21). For the former trajectories the approximation that the effective surface mass in the Baule model is equal to the mass of the surface atom will therefore be better than for in the scattered trajectories. In the latter, the effective surface mass that one should use to calculate the mass ratio may be a factor of 2 to 3 higher for molecules

scattering off bridge and hollow sites. If the Modified Baule model with M_S equal to the mass of a surface atom is applicable to the reactive collision, the difference in energy transfer between PBE and SRP32-vdW (6.6 kJ/mol) accounts for approximately half the energy shift between the associated sticking curves (13.9 kJ/mol).

IV. Summary

The SRP32-vdW and PBE functionals both predict the same activation barrier for the dissociation of CHD_3 on Pt(111), but AIMD trajectory calculations using the PBE functional give a significantly higher sticking coefficient than calculations using the SRP32-vdW functional. The PBE results are also larger than values determined experimentally, which the SRP32-vdW functional reproduces within chemical accuracy[39]. We suggest that the reasons that the two functionals predict such different reactivity are related to the presence of van der Waals correlation in the SRP32-vdW functional, which is absent from the PBE functional. The resultant van der Waals well accelerates the CHD_3 trajectories towards the surface in the case that the SRP32-vdW functional is used, meaning the molecule has less time to distort towards the transition state geometry. It also leads to more energy being transferred from the molecule to the surface, resulting in a lower reactivity. However, we do not find any evidence that the van der Waals well leads to more efficient translational to vibrational energy transfer in the SRP32-vdW trajectories compared to the PBE trajectories, or that the SRP32-vdW potential energy surface is more energetically corrugated than the PBE potential energy surface. Whilst both these factors could lead to a decrease in the reactivity of the SRP32-vdW trajectories compared to the PBE trajectories, neither appears to make a considerable contribution to the difference in reactivity that we observe.

Supplementary Material

See supplementary material for a discussion of the pseudopotentials used in the calculations, analysis of the shape of the potential energy surface and comparison of properties averaged over trajectories.

Acknowledgments

This work was supported financially by the European Research Council through an ERC2013 advanced grant (Nr. 338580), by the Swiss National Science Foundation (Nr. P300P2-171247), and with computer time granted by NWO-EW.

REFERENCES

[1] I. Chorkendorff and J.W. Niemantsverdriet, *Concepts of Modern Catalysis and Kinetics* (Wiley-VCH, Weinheim, 2003).

[2] H. Chadwick and R.D. Beck, Chem. Soc. Rev. **45**, 3576 (2016).

[3] H. Chadwick and R.D. Beck, Annu. Rev. Phys. Chem. **68**, 39 (2017).

[4] R.D. Beck and A.L. Utz, in *Dynamics of. Gas-Surface Interactions Atomic-Level Understanding of Scattering Processes at Surfaces*, edited by R. Dâiez Muiäno and H.F. Busnengo (Springer, Berlin, 2013).

[5] L.B.F. Juurlink, D.R. Killelea, and A.L. Utz, Prog. Surf. Sci. **84**, 69 (2009).

[6] P.M. Hundt, H. Ueta, M.E. van Reijzen, B. Jiang, H. Guo, and R.D. Beck, J. Phys. Chem. A **119**, 12442 (2015).

[7] R.R. Smith, D.R. Killelea, D.F. DelSesto, and A.L. Utz, Science **304**, 992 (2004).

[8] R.D. Beck, P. Maroni, D.C. Papageorgopoulos, T.T. Dang, M.P. Schmid, and T.R. Rizzo, Science **302**, 98 (2003).

[9] P.M. Hundt, M.E. van Reijzen, H. Ueta, and R.D. Beck, J. Phys. Chem. Lett. **5**, 1963 (2014).

[10] D.R. Killelea, V.L. Campbell, N.S. Shuman, and A.L. Utz, Science **319**, 790 (2008).

[11] L. Chen, H. Ueta, R. Bisson, and R.D. Beck, Faraday Discuss. **157**, 285 (2012).

[12] B.L. Yoder, R. Bisson, and R.D. Beck, Science **329**, 553 (2010).

[13] B.L. Yoder, R. Bisson, P.M. Hundt, and R.D. Beck, J. Chem. Phys. **135**, 224703 (2011).

[14] H. Chadwick, H. Guo, A. Gutiérrez-González, J.P. Menzel, B. Jackson, and R.D. Beck, J. Chem. Phys. **148**, 14701 (2018).

[15] S.B. Donald and I. Harrison, Phys. Chem. Chem. Phys. **14**, 1784 (2012).

[16] A. Lozano, X.J. Shen, R. Moiraghi, W. Dong, and H.F. Busnengo, Surf. Sci. **640**, 25 (2015).

[17] B. Jiang, M. Yang, D. Xie, and H. Guo, Chem. Soc. Rev. **45**, 3621 (2016).

[18] H. Guo and B. Jiang, Acc. Chem. Res. **47**, 3679 (2014).

[19] S. Nave, A.K. Tawari, and B. Jackson, J. Phys. Chem. A **118**, 9615 (2014).

[20] H. Guo and B. Jackson, J. Phys. Chem. C **119**, 14769 (2015).

[21] F. Nattino, H. Ueta, H. Chadwick, M.E. van Reijzen, R.D. Beck, B. Jackson, M.C. van Hemert, and G.J. Kroes, J. Phys. Chem. Lett. **5**, 1294 (2014).

[22] F. Nattino, D. Migliorini, G.J. Kroes, E. Dombrowski, E.A. High, D.R. Killelea, and A.L. Utz, J. Phys. Chem. Lett. **7**, 2402 (2016).

[23] R. Peverati and D.G. Truhlar, Philos. Trans. R. Soc. A Math. Phys. Eng. Sci. **372**, 20120476 (2014).

[24] K. Golibrzuch, N. Bartels, D.J. Auerbach, and A.M. Wodtke, Annu. Rev. Phys. Chem. **66**, 399 (2015).

[25] G.J. Kroes, Phys. Chem. Chem. Phys. **14**, 14966 (2012).

[26] C. Díaz, E. Pijper, R.A. Olsen, H.F. Busnengo, D.J. Auerbach, and G.J. Kroes, Science **326**, 832 (2009).

[27] J.P. Perdew, K. Burke, and M. Ernzerhof, Phys. Rev. Lett. **78**, 1396 (1997).

[28] J.P. Perdew, J.A. Chevary, S.H. Vosko, K.A. Jackson, M.R. Pederson, D.J. Singh, and C. Fiolhais, Phys. Rev. B **46**, 6671 (1992).

[29] B. Hammer, L.B. Hansen, and J.K. Nørskov, Phys. Rev. B **59**, 7413 (1999).

[30] L. Sementa, M. Wijzenbroek, B.J. van Kolck, M.F. Somers, A. Al-Halabi, H.F. Busnengo, R.A. Olsen, G.J. Kroes, M. Rutkowski, C. Thewes, N.F. Kleimeier, and H. Zacharias, J. Chem. Phys. **138**, 44708 (2013).

[31] P.M. Hundt, B. Jiang, M.E. van Reijzen, H. Guo, and R.D. Beck, Science **344**, 504 (2014).

[32] F. Nattino, C. Díaz, B. Jackson, and G.J. Kroes, Phys. Rev. Lett. **108**, 236104 (2012).

[33] P. Nieto, D. Farías, R. Miranda, M. Luppi, E.J. Baerends, M.F. Somers, M.J.T.C. van der Niet, R.A. Olsen, and G.J. Kroes, Phys. Chem. Chem. Phys. **13**, 8583 (2011).

[34] I.M.N. Groot, H. Ueta, M.J.T.C. van der Niet, A.W. Kleyn, and L.B.F. Juurlink, J. Chem. Phys. **127**, 244701 (2007).

[35] M. Wijzenbroek and G.J. Kroes, J. Chem. Phys. **140**, 84702 (2014).

[36] F. Nattino, D. Migliorini, M. Bonfanti, and G.J. Kroes, J. Chem. Phys. **144**, 044702 (2016).

[37] C. Diaz, R.A. Olsen, D.J. Auerbach, and G.J. Kroes, Phys. Chem. Chem. Phys. **12**, 6499 (2010).

[38] M. Dion, H. Rydberg, E. Schröder, D.C. Langreth, and B.I. Lundqvist, Phys. Rev. Lett. **92**, 246401 (2004).

[39] D. Migliorini, H. Chadwick, F. Nattino, A. Gutiérrez-González, E. Dombrowski, E.A. High, H. Guo, A.L. Utz, B. Jackson, R.D. Beck, and G.J. Kroes, J. Phys. Chem. Lett. **8**, 4177 (2017).

[40] Y. Matsumoto, Y.A. Gruzdkov, K. Watanabe, and K. Sawabe, J. Chem. Phys. **105**, 4775 (1996).

[41] C. Díaz and R.A. Olsen, J. Chem. Phys. **130**, 94706 (2009).

[42] P.M. Holmblad, J. Wambach, and I. Chorkendorff, J. Chem. Phys. **102**, 8255 (1995).

[43] C.T. Rettner, H.E. Pfnür, and D.J. Auerbach, J. Chem. Phys. **84**, 4163 (1986).

[44] J.H. Larsen, P.M. Holmblad, and I. Chorkendorff, J. Chem. Phys. **110**, 2637 (1999).

[45] A.C. Luntz, J. Chem. Phys. **102**, 8264 (1995).

[46] G. Kresse and J. Hafner, Phys. Rev. B **47**, 558 (1993).

[47] G. Kresse and J. Hafner, Phys. Rev. B **49**, 14251 (1994).

[48] G. Kresse and J. Furthmüller, Phys. Rev. B **54**, 11169 (1996).

[49] G. Kresse and J. Furthmüller, Comp. Mater. Sci. **6**, 15 (1996).

[50] G. Kresse and D. Joubert, Phys. Rev. B **59**, 1758 (1999).

[51] P.E. Blöchl, Phys. Rev. B **50**, 17953 (1994).

[52] V.L. Campbell, N. Chen, H. Guo, B. Jackson, and A.L. Utz, J. Phys. Chem. A **119**, 12434 (2015).

[53] A.K. Tiwari, S. Nave, and B. Jackson, J. Chem. Phys. **132**, 134702 (2010).

[54] H. Guo, A. Farjamnia, and B. Jackson, J. Phys. Chem. Lett. **7**, 4576 (2016).

[55] R. Moiraghi, A. Lozano, and H.F. Busnengo, J. Phys. Chem. C **120**, 3946 (2016).

[56] X. Shen, Z. Zhang, and D.H. Zhang, Phys. Chem. Chem. Phys. **17**, 25499 (2015).

[57] S. Nave, A.K. Tiwari, and B. Jackson, J. Chem. Phys. **132**, 54705 (2010).

[58] S. Nave, A.K. Tawari, and B. Jackson, J. Phys. Chem. A **118**, 9615 (2014).

[59] S. Nave and B. Jackson, J. Chem. Phys. **130**, 54701 (2009).

[60] E.A. McCullough and R.E. Wyatt, J. Chem. Phys. **51**, 1253 (1969).

[61] R.A. Marcus, J. Chem. Phys. **45**, 4493 (1966).

[62] R.D. Levine, *Molecular Reaction Dynamics* (Cambridge University Press, Cambridge, 2005).

[63] B. Baule, Ann. Phys. **349**, 145 (1914).

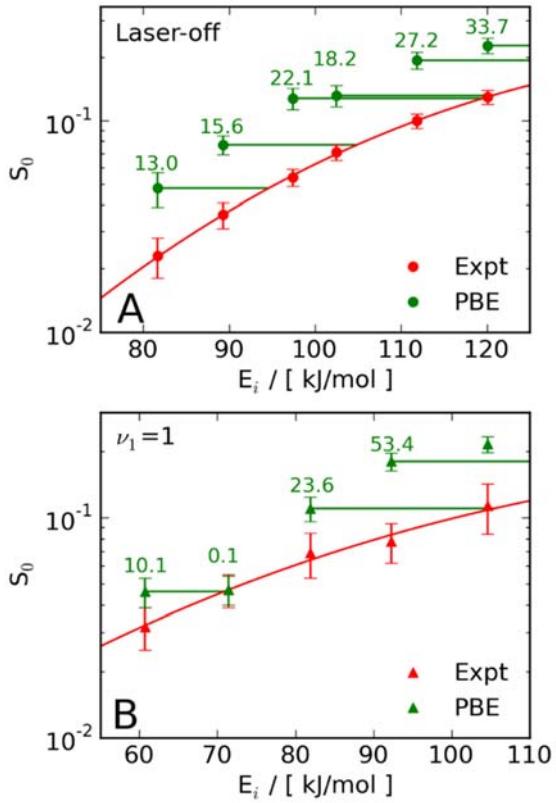

FIG 1. Comparison of the experimentally measured sticking coefficients[39] (red) with those calculated using the PBE functional (green) for CHD_3 dissociation on Pt(111) under laser-off conditions (A) and for molecules prepared with a single quantum of C-H stretch vibration (B). The numbers in the plots are the energy shift in kJ/mol between S_0 calculated with the PBE functional and the fit to the experimental data.

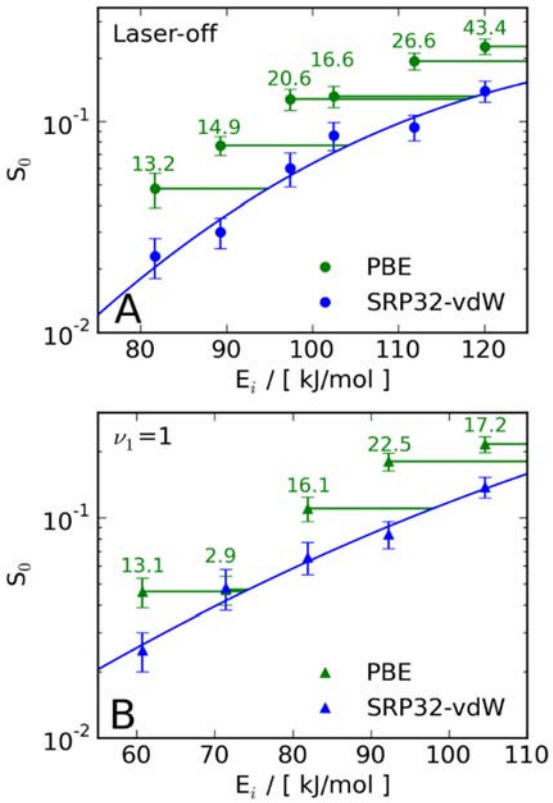

FIG. 2. Comparison of the sticking coefficients calculated using the PBE functional (green) and the SRP32-vdW functional[39] (blue) for CHD_3 dissociation on Pt(111) under laser-off conditions (A) and for molecules prepared with a single quantum of C-H stretch vibration (B). The numbers in the plots are the energy shift in kJ/mol between S_0 calculated with the PBE functional and the fit to the SRP32-vdW data.

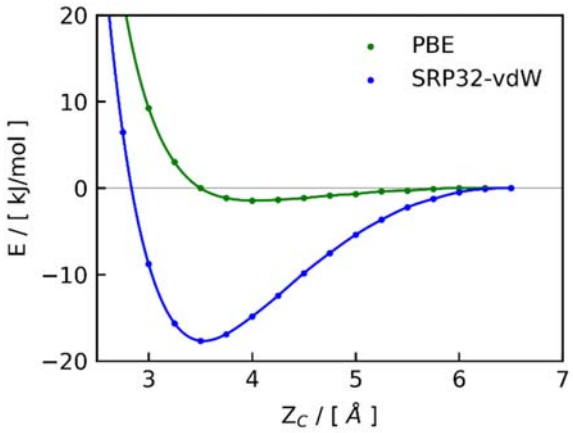

FIG 3. One dimensional cuts through the SRP32-vdW (blue) and PBE (green) PESs showing the difference in van der Waals well obtained with the two functionals. The energy is reported as a function of the distance between the carbon atom and the surface (Z_C) for the molecule with three hydrogen atoms pointing towards the slab.

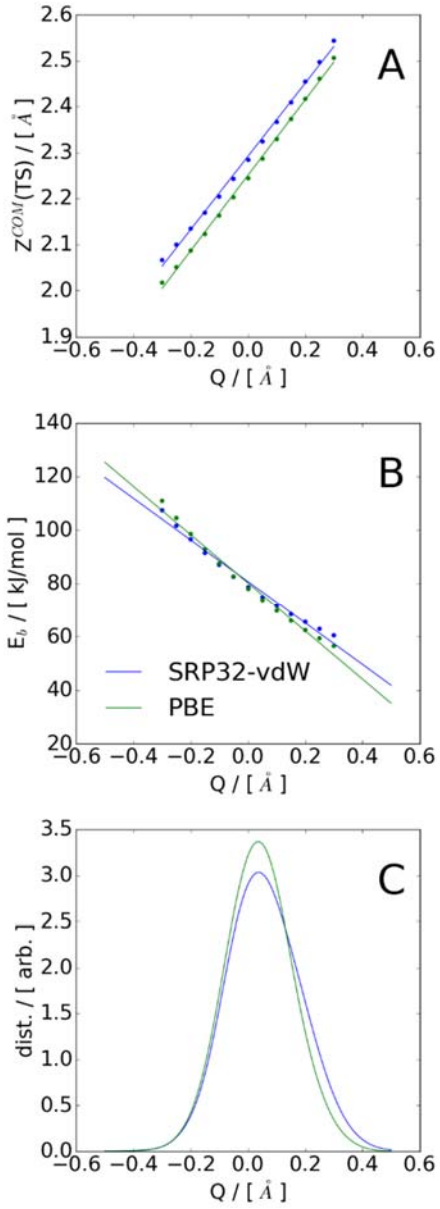

FIG. 4. Panel A: The variation of the height of the molecule's center of mass of the transition state above the surface as a function of the displacement of the surface atom (the mechanical coupling) from the Pt(111) surface for PBE (green) and SRP32-vdW (blue) functionals. The straight lines are fits to the data. Panel B: The variation in the activation barrier height as a function of the displacement of the surface atom (the electronic coupling) from the Pt(111) surface for the PBE (green) and SRP32-vdW (blue) functionals. The straight lines are fits to the data. Panel C: The distribution of the surface atom displacements averaged over the AIMD slabs at a surface temperature of 500 K for the PBE (green) and SRP32-vdW (blue) functionals.

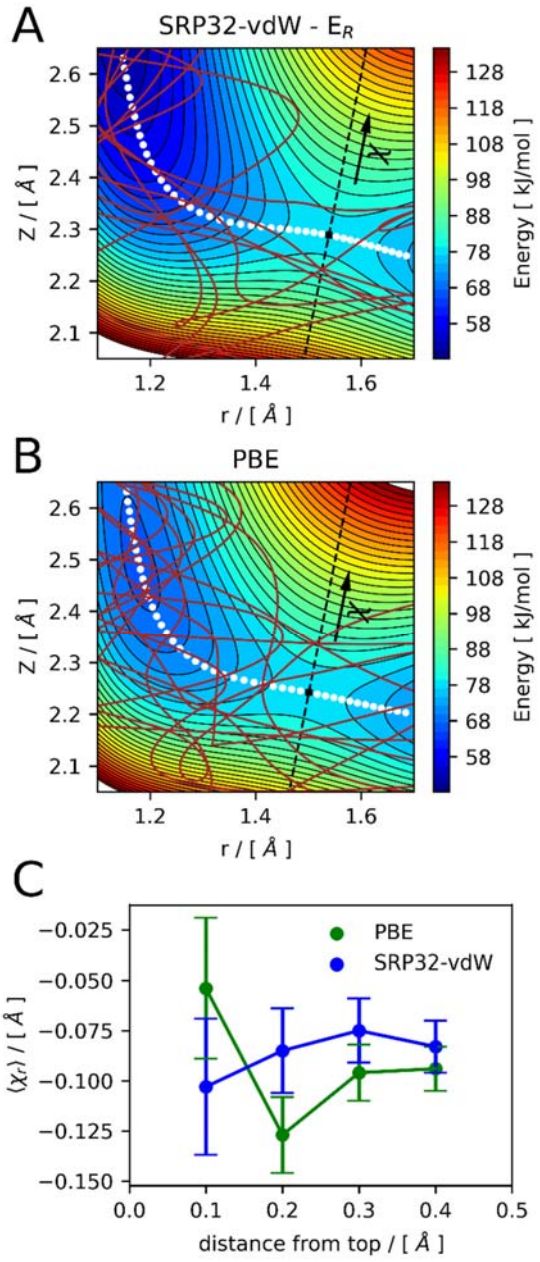

FIG 5. Two dimensional cuts through the SRP32-vdW (A) and PBE (B) potential energy surfaces showing the transition state (black square), minimum energy path (white dotted line) and the vector perpendicular to the minimum energy path (χ, black dashed line). Trajectories that start within 0.1 Å of a top site are also shown (brown lines). All molecular co-ordinates except Z and r have been fixed at the TS values. Panel C: The average distance between the transition state and where the reacted trajectories cross the vector perpendicular to the minimum energy path calculated using Eq. (6) for different distances from a top site for the PBE (green) and SRP32-vdW (blue) trajectories.

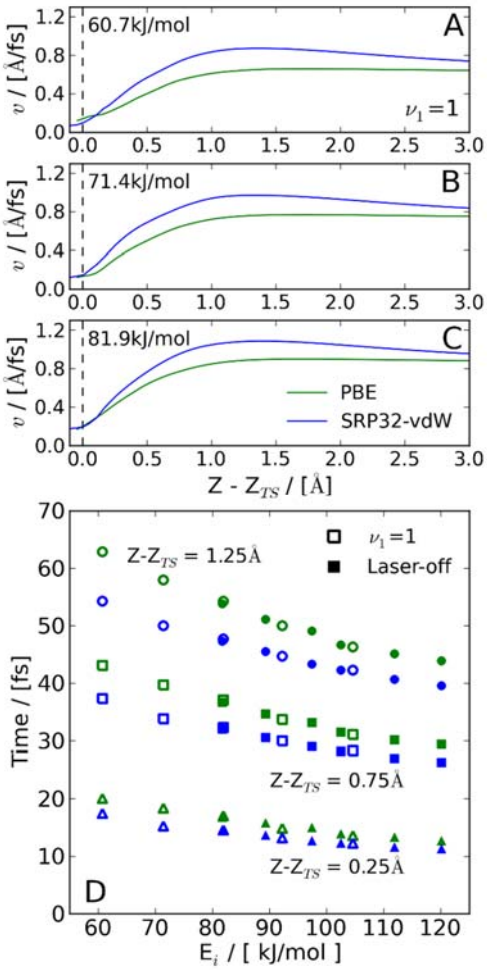

FIG 6. The average velocity of the PBE (green) and SRP32-vdW (blue) trajectories that react as they approach the surface at an incident energy of 60.7 kJ/mol (A), 71.4 kJ/mol (B) and 81.9 kJ/mol (C) with a quantum of initial C-H stretch excitation. The dashed vertical line shows the position of the transition state. Panel D: The average time it takes for the scattered trajectories to travel a distance ΔZ of 1.25 Å (circles), 0.75 Å (squares) and 0.25 Å (triangles) along Z to Z_{TS} for the PBE trajectories (green) and the SRP32-vdW trajectories (blue). The open symbols show the times for the trajectories prepared with a quantum of C-H stretch, and the filled symbols the laser-off trajectories.

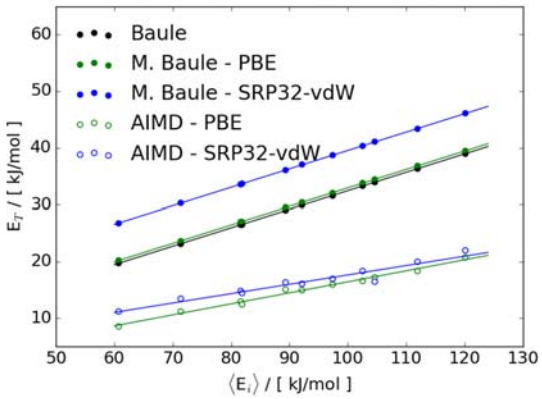

FIG 7. Comparison of the energy transferred to the surface from the AIMD trajectories using the PBE functional (open green symbols) and the SRP32-vdW functional (open blue symbols) with that predicted by the Baule model (black filled symbols) and the Modified Baule model (filled green and blue symbols for PBE and SRP32-vdW respectively). The lines are fits to the data.